

# Implementation of the SCC-DFTB Method for Hybrid QM/MM Simulations within the Amber Molecular Dynamics Package<sup>†</sup>

Gustavo de M. Seabra,<sup>‡</sup> Ross C. Walker,<sup>§,⊥</sup> Marcus Elstner,<sup>||</sup> David A. Case,<sup>§</sup> and Adrian E. Roitberg<sup>\*,‡</sup>

Department of Chemistry and Quantum Theory Project, University of Florida, P.O. Box 118435, Gainesville, Florida 32611-8435, Department of Molecular Biology, TPC15, The Scripps Research Institute, 10550 N. Torrey Pines Road, La Jolla, California 92037, and Institut für Physikalische und Theoretische Chemie, Technische Universität Braunschweig, Hans-Sommer-Strasse 10, D-38106 Braunschweig, Germany

Received: January 4, 2007; In Final Form: April 3, 2007

Self-consistent charge density functional tight-binding (SCC-DFTB) is a semiempirical method based on density functional theory and has in many cases been shown to provide relative energies and geometries comparable in accuracy to full DFT or ab initio MP2 calculations using large basis sets. This article shows an implementation of the SCC-DFTB method as part of the new QM/MM support in the AMBER 9 molecular dynamics program suite. Details of the implementation and examples of applications are shown.

## Introduction

Computational studies are important for understanding biologically relevant systems such as proteins, nucleic acids, and carbohydrates. Those systems are usually too large to be treated with quantum mechanical (QM) methods, and approximated molecular mechanics (MM) methods based on classical mechanics such as Monte Carlo (MC) or molecular dynamics (MD) are used instead.<sup>1</sup> These MM methods apply parametrized force fields to describe molecular properties such as bond lengths, angles, dihedrals, electrostatic, and van der Waals forces. The use of such parametrized methods reduces the computational complexity sufficiently to allow for the study of processes including ligand binding,<sup>2,3</sup> enzyme reaction mechanisms,<sup>4</sup> protein folding,<sup>5</sup> refolding,<sup>6</sup> and denaturation,<sup>7</sup> providing invaluable help in the analysis of complex experimental data and structures.

Among the computational packages developed for MM calculations, one of the most commonly used for MD simulations of biological systems is the AMBER package.<sup>8</sup> “AMBER” is an acronym to assisted model building with energy refinement, a name that reflects its origins in the late 1970s and actually refers to a suite of programs (rather than a single program) developed to carry out and analyze MD simulations providing a powerful framework particularly for simulations of biologically relevant systems such as proteins, nucleic acids, and carbohydrates.<sup>8</sup> The name AMBER is also often used to refer to the particular family of force fields implemented in the AMBER package, although the proper reference to the force field should include specific version details (e.g., ff99).

Despite continuous efforts to develop more reliable force fields for use in such calculations,<sup>9</sup> including the use of QM calculations and genetic algorithms in the parametrization of the force field, classical mechanics methods lack the ability to treat fundamentally quantum processes, such as bond breaking and forming and charge fluctuations as a function of geometry,<sup>10</sup> or to describe parts of the potential energy surface far from equilibrium.<sup>11</sup> In some cases, although computationally expensive, it is possible to treat a model system purely by QM methods,<sup>12,13</sup> but the effect of the environment must be either neglected or simulated by a continuum dielectric approximation. An alternative that allows the explicit inclusion of environment effects while treating the most relevant part of the system with full quantum mechanics was first explored by Warshel and Levitt as early as 1976<sup>14</sup> and is the use of hybrid quantum mechanics/molecular mechanics (QM/MM) calculations whereby a subsection of the system is treated by QM methods, the remainder (environment) is treated by standard molecular mechanics (MM) methods, and a coupling potential is used to connect the two regions.<sup>15</sup>

In its latest incarnation (version 9),<sup>16</sup> AMBER includes significantly improved QM/MM support (as compared to earlier versions of AMBER), with seamless integration in its MD program, SANDER. (The acronym refers to simulated annealing with NMR derived energy restraints but, since its first version, the program has evolved to perform many tasks completely unrelated to NMR.) This new QM/MM module supports a variety of semiempirical QM Hamiltonians such as MNDO,<sup>17,18</sup> AM1,<sup>19</sup> PM3,<sup>20,21</sup> PM3/PDDG,<sup>22</sup> MNDO/PDDG,<sup>22</sup> MNDO/d,<sup>23</sup> and SCC-DFTB.<sup>24,25</sup> This manuscript refers specifically to the implementation of the SCC-DFTB method in AMBER, while the implementation of the other QM methods along with support for generalized Born and the development of a QM/MM compatible particle-mesh Ewald treatment of long-range electrostatics are discussed in a separate article.<sup>26</sup>

## Theory

**Molecular Mechanics.** As mentioned before, in a MM calculation, a parametric equation is used to describe the

<sup>†</sup> Part of the “DFTB Special Section”.

<sup>\*</sup> To whom correspondence should be addressed. E-mail: roitberg@ufl.edu.

<sup>‡</sup> Department of Chemistry and Quantum Theory Project, University of Florida.

<sup>§</sup> Department of Molecular Biology, TPC15, The Scripps Research Institute.

<sup>||</sup> Institut für Physikalische und Theoretische Chemie, Technische Universität Braunschweig.

<sup>⊥</sup> Current address: San Diego Supercomputer Center, University of California San Diego, 9500 Gilman Drive, La Jolla, CA 92093-0505.

energetics of the system. A simple functional preserving the essential nature of molecules in condensed phases is used in SANDER:

$$U(\mathbf{R}) = \sum_{\text{bonds}} K_r (r - r_{\text{eq}})^2 + \sum_{\text{angles}} K_\theta (\theta - \theta_{\text{eq}})^2 + \sum_{\text{dihedrals}} \frac{V_n}{2} [1 + \cos(n\phi - \gamma)] + \sum_{A < B}^{\text{atoms}} \left( \frac{A_{AB}}{R_{AB}^{12}} - \frac{B_{AB}}{R_{AB}^6} \right) + \sum_{A < B}^{\text{atoms}} \frac{Q_A Q_B}{\epsilon R_{AB}} \quad (1)$$

The terms in the right-hand side represent the bond, angle, dihedral, van der Waals, and electrostatic potential energies, respectively. To run a MM calculation, the parameters  $K_r$ ,  $r_{\text{eq}}$ ,  $K_\theta$ ,  $\theta_{\text{eq}}$ ,  $V_n$ ,  $\gamma$ ,  $A_{AB}$ ,  $B_{AB}$ , and the charges  $Q_A$  must be adjusted for different molecules or residues, usually to reproduce some experimental property or quantum calculation. The term “force field” refers to a specific set of those parameters, derived to work together.

Part of the difficulties encountered by MM simulations comes from the quadratic nature of the two first terms, which forbids bond breaking to occur. Also, effects due to electronic rearrangement are neglected by fixing the charges. This last hurdle can be partially overcome by the use of polarizable force fields,<sup>27,28</sup> however at an increased computational cost. Another alternative is the use of hybrid QM/MM methods, as discussed below.

**QM/MM.** In a hybrid QM/MM calculation,<sup>14,15</sup> the system is partitioned into two regions: a QM region, typically consisting of a relatively small number of atoms relevant for the specific process being studied, and a MM region with all the remaining atoms. The total Hamiltonian ( $\hat{H}$ ) for such a system is written as:

$$\hat{H} = \hat{H}^{\text{QM}} + \hat{H}^{\text{MM}} + \hat{H}^{\text{QM/MM}} \quad (2)$$

where  $\hat{H}^{\text{QM}}$  and  $\hat{H}^{\text{MM}}$  are the Hamiltonians for the QM and MM parts of the system and are calculated using either the QM method chosen or the usual force field equations, respectively. The remaining term,  $\hat{H}^{\text{QM/MM}}$ , describes the interaction between the QM and MM parts and typically contains terms for electrostatic, van der Waals, and bonded interactions across the region boundaries:

$$\hat{H}^{\text{QM/MM}} = \hat{H}_{\text{vdW}}^{\text{QM/MM}} + \hat{H}_{\text{elect}}^{\text{QM/MM}} + \hat{H}_{\text{bonds}}^{\text{QM/MM}} \quad (3)$$

In AMBER’s SCC-DFTB implementation, the electrostatic interaction energy between QM and MM regions is calculated as a Coulomb interaction between the atomic charges ( $q_\alpha$ ), derived from the SCC-DFTB by means of Mulliken population analysis and the parametrized (RESP) charges of the MM atoms ( $Q_A$ ) from the classical force field:

$$E_{\text{elect}}^{\text{QM/MM}} = \sum_{\alpha}^{\text{QM}} \sum_A^{\text{MM}} \frac{Q_A q_\alpha}{r_{\alpha A}} \quad (4)$$

where  $r_{\alpha A}$  is the distance between the QM atom  $\alpha$  and the MM atom  $A$  (Greek letters are used here for QM atoms, and roman for MM atoms). This interaction is added as an extra term to the SCC-DFTB Hamiltonian, and the energy of the quantum system in the presence of the MM external charges is calculated via the self-consistent process described below.

The  $\hat{H}_{\text{vdW}}^{\text{QM/MM}}$  term is calculated as usual, using the standard 12–6 Lennard-Jones equation and parameters derived from the

force field in use for both the QM and MM atoms. It has been shown that the use of the MM parameters in this interaction does not introduce significant errors in the calculation.<sup>29</sup>

$$E_{\text{vdW}}^{\text{QM/MM}} = \sum_{\alpha}^{\text{QM}} \sum_A^{\text{MM}} \left[ \frac{A_{\alpha A}}{R_{\alpha A}^{12}} - \frac{B_{\alpha A}}{R_{\alpha A}^6} \right] \quad (5)$$

Finally, if there are covalent bonds across the boundaries of the QM/MM system, additional approximations are necessary. The way in which one should treat covalent bonds that cross the QM–MM interface is probably the most debated subject in hybrid QM/MM simulations, and a variety of different methods have been proposed for dealing with this problem. Broadly the most commonly utilized methods fall into three categories. The first category, and the approach used in AMBER, is the link atom approach. First introduced by Singh and Kollman,<sup>30</sup> this method has found widespread use in QM/MM calculations, with a number of variations being developed later, including those by Bersuker et al.<sup>31</sup> and Morokuma et al.<sup>32</sup> In this approach, a link atom, which is typically but not always a hydrogen atom, is placed along the bond between the QM and MM region at a suitable distance ( $\sim 1$  Å) to satisfy valence requirements. The link atom is included in the QM part of the calculation as a regular QM atom. It shares the same pair list for QM–MM interactions as real QM atoms. Such an approach does nothing to maintain the bond between the QM and MM regions, and so this must be dealt with classically in the MM part of the calculation.

The second category of methods are the capping potential or pseudo bond methods,<sup>33</sup> which use an element of fictitious type to “cap” each bond between the QM and MM regions. The third category is the hybrid-orbital approach, which employs either hybrid or localized frozen orbitals on the QM atom of the QM–MM covalent pair.<sup>34,35</sup>

The link atom approach is by far the simplest to implement and, if used carefully, can give satisfactory results.<sup>36</sup> A recent study by König et al. on the effect of different QM/MM frontier treatments with SCC-DFTB as the QM method also concluded that the effect of using different link atom schemes in QM/MM simulations is rather small, especially in reactions that conserve the total charge, and emphasizes that other technical details such as the treatment of long-range electrostatics can often play a more important role.<sup>37</sup>

There are a number of ways to implement a link atom approach that deal with both the way the link atom is positioned, the way the forces on the link atom are propagated, and the way nonbonding interactions around the link atom are treated. For DFTB calculations, we use a link atom scheme developed as part of the rewriting of AMBER’s semiempirical QM/MM method is used.<sup>26</sup> This approach is similar to that used by Dynamo,<sup>36</sup> where the link atom is treated as part of the covalent bond between the QM and MM atoms bonded across the interface. Each time an energy or gradient calculation is to be done, the link atom coordinates are automatically generated from the current coordinates of the QM and MM atoms making up the QM–MM covalent pair. The link atom is placed along the bond vector joining the QM and MM atom using the formula:

$$\bar{r}_L = \bar{r}_{\text{QM}} + d_{L-\text{QM}} \frac{\bar{r}_{\text{MM}} - \bar{r}_{\text{QM}}}{|\bar{r}_{\text{MM}} - \bar{r}_{\text{QM}}|} \quad (6)$$

where  $\bar{r}_L$ ,  $\bar{r}_{\text{QM}}$ , and  $\bar{r}_{\text{MM}}$  are the position vectors of the link atom, QM atom, and MM atom, respectively, and  $d_{L-\text{QM}}$  is a user-defined constant specifying the QM to link atom bond length. By default,  $d_{L-\text{QM}}$  is set to the equilibrium distance of a methyl

C–H atom pair (1.09 Å), but this can be changed at run time if desired. Similarly, while the default link atom to be used is a hydrogen atom, this can be changed by the user at run time as necessary.

The electrostatic interactions of the MM link pair atom are replaced by those of the link atom, while the van der Waals interactions remain with the MM link pair atom. This is achieved by zeroing the charge of this MM atom for the entire duration of the MD simulation such that all other atoms that would normally see this atom's charge instead see the link atom, which has no van der Waals radius. The link atom position is calculated at each dynamics step based on the current positions of the QM–MM link pair. Once the link atom position is known, it can be employed in the quantum part of the energy evaluation. The link atom is treated in exactly the same way as the real QM atoms. It shares the same nonbond list as the other QM atoms interacting with the point charges of the MM atoms. Test calculations have shown that this approach gives significantly better stability of the charge on QM atoms around the QM–MM interface than is observed if the QM link atom interacts only with other QM atoms not seeing the MM charge field.<sup>26</sup> In addition, while our link atom approach introduces a slight displacement in position of the charge on the MM link atom to a dynamic charge on the link atom, the overall effect is likely to be very minor. Also, the gradients are formally correctly dealt with when transferring the force on the QM link atom back to the atoms making up the QM–MM link pair and so this approach properly conserves energy. We feel that it is more important to concentrate on improving the accuracy of the QM Hamiltonian and the size of QM system that can be simulated in a given time than at it is to overly tweak the treatment of covalent bonds. Such an approach is also advocated by other QM/MM software developers.<sup>36</sup>

Once the QM gradient has been calculated, the force on each link atom is redistributed between the QM and MM link pair by application of the chain rule.

There are a number of advantages to this link atom approach. The first is that constraining the link atom position to the QM–MM link pair bond vector does not introduce extra degrees of freedom into the calculation. This makes temperature and pressure control easier and also means that statistical averages and fluctuations can be directly compared between pure MM and hybrid QM/MM simulations. The second is that the entire link atom procedure is transparent to the user. The user simply selects which atoms are to be treated quantum-mechanically, and the code then determines which bonds are to be broken, how many link atoms are needed, and where they are to be placed. The third is that the link atom position need only be known by the QM part of the code, and as such there is no need for special restart file formats or extension of the coordinate, force, or velocity arrays. This makes the implementation significantly easier and greatly reduces the potential for coding errors. A fourth and very desirable advantage is that the definition of the link atom position (eq 6) ensures that the link atom is always in the correct position each time the QM potential is calculated. Our experience shows that this greatly improves the convergence behavior and stability of QM/MM MD simulations and allows time steps of the same magnitude as are typically used in classical MD simulations.

The remaining details of how the QM–MM boundary is treated are as follows: for the interactions surrounding the link atom, the MM bond term between the QM and MM atom are calculated classically using the AMBER force field parameters as are any angle or dihedral term that include at least one MM

atom. The Lennard-Jones interactions between QM–MM atom pairs are calculated in the same way as described in the section above with exclusion of 1–2 and 1–3 interactions and scaling of 1–4 interactions in line with the ethos of the AMBER force field. This just leaves the electrostatic interactions between QM and MM atoms around the region of the link atom. For this, a number of approaches was investigated.<sup>26</sup> The best method found is one where all electrostatic interactions between any MM atom (excluding MM atoms directly bonded to a QM atom) that is within the user specified cutoff distance of any QM atom are calculated for all QM atoms, including the link atom, without exclusion or scaling. This method overestimates the interactions of 1–2, 1–3, and 1–4 QM–MM atom pairs due to the fact that these interactions are included in the bond, angle, and dihedral parametrization and in the QM calculation. However, while not always the optimum method, it is simple to implement and experience has shown that it behaves well in the widest variety of situations.<sup>26</sup>

Charge conservation with link atoms is achieved by one of two methods. Any difference in charge between the QM region and the parametrized charges of the MM atoms that are replaced by QM atoms can either be distributed to the MM atoms surrounding the MM link atom pair or evenly across all the remaining MM atoms. This approach is discussed in more detail elsewhere.<sup>26</sup>

**SCC-DFTB.** The self-consistent charge density functional tight-binding (SCC-DFTB) method is an approximate method based on density functional theory (DFT). The SCC-DFTB theory has been described in detail elsewhere<sup>24,25</sup> (and in other articles in this issue), therefore only a short summary will be presented here.

In the SCC-DFTB approximation, the electronic density in DFT theory is substituted by a reference density plus fluctuations,  $\rho = \rho_0(r) + \delta\rho(r)$ . The DFT total energy is then expanded up to second-order terms in the charge density fluctuations. After some approximations, the result can be written in a tight-binding format as:<sup>25</sup>

$$E^{\text{SCC-DFTB}} = \sum_i^{\text{occ}} \langle \psi_i | \hat{H}_0 | \psi_i \rangle + E_{\text{rep}} + \frac{1}{2} \sum_{\alpha\beta} \Delta q_\alpha \Delta q_\beta \gamma_{\alpha\beta} \quad (7)$$

The two first terms on the right-hand side of eq 7 are calculated at the reference density  $\rho_0$  and form the original (non-self-consistent charge or first order) DFTB approximation.<sup>38</sup> The first term is the “band structure term” (this terminology is inherited from the materials science origins of the DFTB approximation) and refers to the leading matrix element of the Hamiltonian,  $\hat{H}_0$ . The Kohn–Sham molecular orbitals  $\psi_i$  are expanded in a minimal basis set of Slater-type confined atomic orbitals, i.e.,  $\psi_i = \sum_{\nu} c_{\nu i} \varphi_\nu$  as described by Eschrig and Bergert,<sup>39</sup> which is determined by solving the atomic Kohn–Sham problem in the presence of a confining potential.<sup>38</sup> These atomic orbitals ( $\varphi_\nu$ ) are then used to calculate the Hamiltonian matrix elements as:

$$H_{\mu\nu}^0 = \begin{cases} \epsilon_\mu^{\text{free atom}} & , \text{ if } \varphi_\mu = \varphi_\nu; \\ \langle \varphi_\mu | \hat{H}(\rho_\alpha^0 + \rho_\beta^0) | \varphi_\nu \rangle & , \varphi_\mu \in \alpha \text{ and } \varphi_\nu \in \beta; \\ 0 & , \text{ otherwise} \end{cases} \quad (8)$$

In eq 8,  $\epsilon_\mu^{\text{free atom}}$  is the Kohn–Sham eigenvalue for orbital  $\varphi_\mu$  in the unconfined atom, and three-center terms have been neglected. The Hamiltonian and overlap matrix elements are then precalculated in this two-center approximation for interatomic distances on a relevant scale and tabulated,<sup>25,38</sup> and

matrix elements at arbitrary distances can be obtained by interpolation from the tables.

The second term is a short-range, pairwise repulsive interaction, approximated as a sum of two-body potentials,

$$E_{\text{rep}} = \sum_{\alpha\beta} U_{\alpha\beta} \quad (9)$$

In practice, this term is fitted (using spline functions) to the difference of total energies between a full DFT calculation and the electronic part of a DFTB calculation (all terms except  $E_{\text{rep}}$ ) with respect to the bond length of interest in a suitable set of reference molecules.<sup>40</sup>

The last term in eq 7 defines the second order, self-consistent charge (SCC) approximation. It introduces long-range Coulomb interaction corrections to the total energy due to the fluctuations in the charges ( $\Delta q_{\alpha} = q_{\alpha} - q_{\alpha}^0$ ) centered at the atoms. The  $\gamma_{\alpha\beta}$  is an analytical function yielding the correct behavior in the limiting cases: for  $R_{\alpha} = R_{\beta}$ ,  $\gamma_{\alpha\beta}$  gives the self-interaction contribution of  $\alpha$ , which evaluates to the Hubbard parameter for atom  $\alpha$  ( $U_{\alpha}$ ), and at the limit of large distances, it is the pure Coulombic interaction between the two spherical charge distributions centered at  $R_{\alpha}$  and  $R_{\beta}$ .

Applying the variational principle, the final Kohn–Sham equations can be written as the system of algebraic equations:

$$\begin{aligned} H_{\mu\nu} &= \langle \varphi_{\mu} | \hat{H}_0 | \varphi_{\nu} \rangle + \frac{1}{2} S_{\mu\nu} \sum_{\xi}^N (\gamma_{\alpha\xi} + \gamma_{\beta\xi}) \Delta q_{\xi} \\ &= H_{\mu\nu}^0 + H_{\mu\nu}^1; \quad \forall \mu \in \alpha, \nu \in \beta \end{aligned} \quad (10)$$

where

$$H_{\mu\nu}^0 = \langle \varphi_{\mu} | \hat{H}_0 | \varphi_{\nu} \rangle; \quad S_{\mu\nu} = \langle \varphi_{\mu} | \varphi_{\nu} \rangle; \quad \forall \mu \in \alpha, \nu \in \beta \quad (11)$$

Therefore, the second-order correction due to charge fluctuations is represented by the nondiagonal  $H_{\mu\nu}^1$  terms, which depend on the atomic charges. These charges are calculated by Mulliken analysis and depend on the coefficients  $c_{\mu i}$  of the Kohn–Sham orbitals. So, the process must be iterated until self-consistency is achieved. Because no integrals need to be calculated, the computational time is dominated by the solution of the eigenvalue problem in eq 10.

Finally, a simple analytic expression for the interatomic forces can be derived by taking the derivative of the SCC-DFTB energy with respect to the nuclear coordinates to yield:

$$\begin{aligned} \mathbf{F}_{\alpha} = & - \sum_i^{\text{occ}} n_i \sum_{\mu\nu} c_{\mu i} c_{\nu i} \left( \frac{\partial H_{\mu\nu}^0}{\partial \mathbf{R}_{\alpha}} - \left( \epsilon_i - \frac{H_{\mu\nu}^1}{S_{\mu\nu}} \right) \frac{\partial S_{\mu\nu}}{\partial \mathbf{R}_{\alpha}} \right) - \\ & \Delta q_{\alpha} \sum_{\xi}^{\text{QM}} \frac{\partial \gamma_{\alpha\xi}}{\partial \mathbf{R}_{\alpha}} \Delta q_{\xi} - \frac{\partial E_{\text{rep}}}{\partial \mathbf{R}_{\alpha}} \end{aligned} \quad (12)$$

The derivatives for the Hamiltonian and overlap are calculated as needed from the tabulated values via a finite differences approach, while simple analytical formulas can be obtained for all of the remaining terms.

**Dispersion.** SCC-DFTB, being an approximation to DFT, inherits many of its limitations. One important such limitation is the well-known fact that the local density approximation (LDA) or generalized gradient approximation (GGA) in DFT functionals do not properly account for dispersion forces.<sup>41,42</sup> Efforts have been made to correct for this behavior as an a posteriori addition to DFTB.<sup>43,44</sup> The method used in the

AMBER implementation follows Elstner et al.,<sup>43</sup> where an empirical correction is applied to the DFTB energy expression to yield:

$$E^{\text{SCC-DFTB/d}} = E^{\text{SCC-DFTB}} - \sum_{\alpha\beta} f(R_{\alpha\beta}) \frac{C_6^{\alpha\beta}}{R_{\alpha\beta}^6} \quad (13)$$

The  $C_6^{\alpha}$  parameters are derived from experimental atomic polarizabilities, and the damping function  $f(R_{\alpha\beta})$  adjusted in order to reproduce a large set of reference data.<sup>43</sup> The damping function used in the AMBER implementation is the same as in Elstner's work:<sup>43</sup>

$$f(R_{\alpha\beta}) = [1 - \exp(-d(R_{\alpha\beta}/R_{\alpha\beta}^0)^N)]^M \quad (14)$$

with the same values of  $d = 3.0$ ,  $N = 7$ , and  $M = 4$  for all atoms and  $R_{\alpha\beta}^0$  calculated by a combination rule:

$$R_{\alpha\beta}^0 = \frac{(R_{\alpha}^0)^3 + (R_{\beta}^0)^3}{(R_{\alpha}^0)^2 + (R_{\beta}^0)^2} \quad (15)$$

using  $R_{\alpha}^0 = 3.5$  Å for H, 3.8 Å for C, N, and O, and 4.8 Å for P and S atoms. The parameters in the original publication were developed for DNA  $\pi$ – $\pi$  stacking interaction<sup>43</sup> but can be adjusted in an atom-by-atom base if needed.

## Implementation

The implementation of SCC-DFTB in AMBER 9 is based on the original DFTB source code (version 26.11.1998). However, the code in AMBER 9 has been extensively rewritten to conform to FORTRAN 95 standards, including full dynamic memory allocation and greatly enhanced performance. It has been integrated in the SANDER program such that just a change of a few keyword values are needed to request a SCC-DFTB calculation with the aim that the method be compatible with as many of the classical MM approaches, such as replica exchange,<sup>45</sup> targeted MD,<sup>46,47</sup> etc. as possible. Some minor modifications to the process of energy and gradient calculations particular to the AMBER implementation are described below. These modifications were done in the spirit of better calculation of forces, resulting in much better energy conservation in constant energy ( $nVE$ ) MD runs. Developing a QM/MM approach that can adequately conserve energy in the  $nVE$  ensemble to approximately the same tolerances as classical MM simulations has been paramount in this work. Details of the ways in which energy conservation has been achieved and why a high degree of accuracy in the forces is required is discussed in detail elsewhere.<sup>26</sup>

The DFTB parameter files needed are the same as distributed with the original DFTB. These files must be obtained separately and are available free of charge from Marcus Elstner or from the DFTB website (<http://www.dftb.org>).

**SCF Convergence.** Generally, the self-consistent-field calculations are considered converged when the energy difference between two consecutive iterations falls below an acceptable threshold. Differing from the other SCC-DFTB implementations, the AMBER implementation requires a second convergence criterion: that the maximum difference between the charges in any atom from two successive iterations also falls below an established tolerance, which is set to either  $0.05 \times (\text{SCF tolerance})^{1/2}$ , the default, or equal to the SCF tolerance, if tighter convergence is needed. This modification adds a very small

```

Example mdin file for sander with SCC-DFTB
&cntrl
  imin =0, maxcyc=50000, ncyc=1000,
  irect=1, ntp=500, ntwx=500, ntwr=1000, iwrap=1,
  ntx=5, ntb=1, cut=7.0,
  ntc=2, ntf=2,
  nstlim=50000000, dt=0.002,
  ntt=0,
  ifqnt=1, igb=0,
/

&qmmm
  qmmask=":1-3",
  qmtheory=7,
  dftb_disper=1,
  dftb_chg=1,
  scfconv=1.0e-9, tight_p_conv=1,
  qm_ewald=1,
/

```

**Figure 1.** Example input file for sander using QM/MM and SCC-DFTB.

number of iterations in the SCF procedure and results in more accurate gradients and better energy conservation during molecular dynamics calculations.

Also, assuming the atomic charges only change slightly from one MD step to the next, the converged charges from the previous MD step can be used as the initial guess in the SCF procedure of the next MD step, resulting in accelerated SCF convergence. This can, however, lead to convergence difficulties when there is a larger change in charges from one MD step to the next, in which case, the initial guess is reset to the default neutral atom values and the SCF process is restarted.

**Gradients.** A second modification made in the AMBER implementation is in the calculation of derivatives in eq 12. Because the Hamiltonian and Overlap matrices are tabulated, their derivatives are calculated by a finite differences algorithm. The original DFTB implementation used a displacement of  $0.01 a_0$  in this process, while a tighter value of  $0.00001 a_0$  is used in AMBER. This tighter value was found to yield more accurate forces when compared to forces calculated by finite differences of the total energy.

**CM3 Charges.** The charge model 3 (CM3) comes from a mapping procedure developed to correct for systematic errors in individual bond dipoles.<sup>48</sup> The procedure is optimized to accurately reproduce charge-dependent properties such as dipole moments and has been shown to provide a more realistic description of the molecular charge distribution. The mapping can be written as:

$$q_{\alpha}^{\text{CM3}} = q_{\alpha}^0 + \sum_{\beta \neq \alpha} T_{\alpha\beta} \quad (16)$$

where the  $q_i^{\text{CM3}}$  and  $q_i^0$  are the CM3 and original (e.g., Mulliken or Löwdin) charges, respectively. The elements of the transfer matrix  $\mathbf{T}$  ( $T_{ij}$ ) are defined based on the Mayer bond order matrix  $\mathbf{B}$  as:

$$T_{\alpha\beta} = D_{Z_{\alpha}Z_{\beta}} B_{\alpha\beta} + C_{Z_{\alpha}Z_{\beta}} B_{\alpha\beta}^2 \quad (17)$$

The elements of the Mayer bond order matrix are defined from the density and overlap ( $\mathbf{P}$  and  $\mathbf{S}$ ) matrices as:

$$B_{\alpha\beta} = \sum_{i \in \alpha} \sum_{j \in \beta} (\mathbf{PS})_{ji} (\mathbf{PS})_{ij} \quad (18)$$

where  $i$  and  $j$  are atomic orbitals centered on the atoms  $\alpha$  and  $\beta$ . The calculation of the CM3 charges has been included in the AMBER implementation based on the parametrization by Kalinowski et al.,<sup>49</sup> which was developed specifically for the SCC-DFTB method as a mapping of the regular Mulliken charges already calculated. The CM3 charges take no part in the SCF process and are calculated only as needed for printout and have no impact in the total computational time.

**Long-Range Electrostatics.** The Ewald sum method<sup>1,50</sup> can be used for the treatment of long-range electrostatics under periodic boundary conditions. In this case, the  $\gamma_{\alpha\beta}$  function of eq 19 is modified to include an Ewald pair potential term ( $\varphi_{\alpha\beta}$ ), which accounts for the QM–QM and QM–MM long-range electrostatics:

$$\gamma_{\alpha\beta}^{\text{Ew}} = \gamma_{\alpha\beta} + \varphi_{\alpha\beta} \quad (19)$$

where  $\varphi_{\alpha\beta} = \varphi_{\alpha\beta}(r_{\alpha\beta})$  is the usual Ewald pair potential between atoms  $\alpha$  and  $\beta$ .<sup>1</sup> This leads to a modified eigenvalue problem (eq 10) that includes the Ewald pair potential:

$$H_{\mu\nu} = \langle \varphi_{\mu} | \hat{H}_0 | \varphi_{\nu} \rangle + \frac{1}{2} S_{\mu\nu} \sum_{\xi}^N (\gamma_{\alpha\xi} + \gamma_{\beta\xi} + \varphi_{\alpha\xi} + \varphi_{\beta\xi}) \Delta q_{\xi} \quad (20)$$

The sum  $\sum_{\xi}^N \varphi_{\alpha\xi} \Delta q_{\xi}$  gives the Ewald field at the position of atom  $\alpha$  and must include terms due to both the QM–QM and QM–MM interactions. Because the MM charges are constant, the latter can be calculated only once outside the SCF, while the former is calculated using the current Mulliken charges at each SCF iteration in order to obtain, at the end of SCF procedure, a set QM charge distribution that is consistent with both the periodic MM field and the periodic QM field.

The AMBER 9 implementation of the Ewald sum for QM/MM calculations is based on a modification of the work by Nam et al.<sup>51</sup> In that work, the authors use the Ewald sum method for treating both the QM–QM and QM–MM interactions, which can be expensive for large MM regions. AMBER 9 includes a new implementation of the FFT based particle-mesh Ewald<sup>52</sup> (PME) method for the QM–MM interactions developed by Walker, Crowley, and Case,<sup>26</sup> which, dependent on system size, is typically 1 to 2 orders of magnitude faster and less memory intensive than the regular Ewald method.

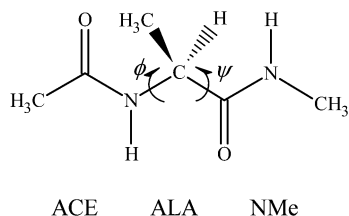


Figure 2. Alanine dipeptide.

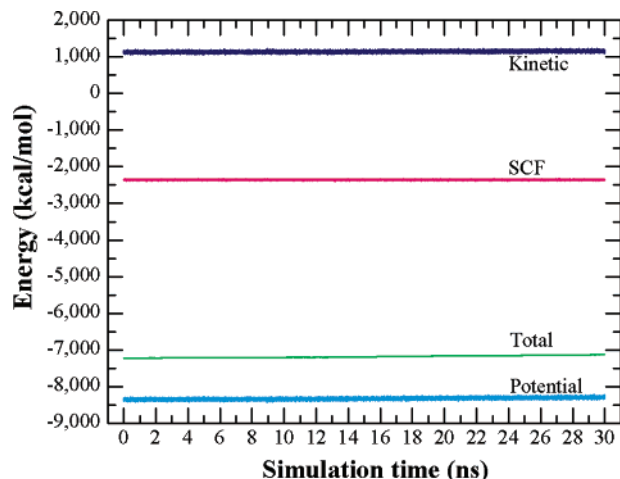


Figure 3. Energies from the QM/MM simulation using  $1.0 \times 10^{-9} E_h$  convergence criteria.

**Implicit Solvent.** An SCC-DFTB parametrization of the generalized Born (GB) method for implicit solvation has been described by Xie and Liu.<sup>53</sup> In this method, a GB polarization term is added to the  $\gamma_{\alpha\beta}$  function resulting in a modified eigenvalue equation, in a very similar manner as described above for the Ewald long-range electrostatic interactions.

AMBER 9 includes support for implicit solvent in QM/MM simulations by the GB method, as described by Pellegrini and Field.<sup>54</sup> Efforts are currently under way to integrate the QM-GB and the SCC-DFTB implementations in AMBER, and details as well as sample applications will be described elsewhere.

**Integration within SANDER.** One of the goals of the current implementation was to provide full integration of the SCC-DFTB method with the MD capabilities of SANDER, AMBER's MD module. As an illustration, Figure 1 shows an input for a QM/MM MD calculation in SANDER using SCC-DFTB as the QM method. The `ifqnt=1` flag in the `&cntrl` namelist specifies that part of the system is to be treated quantum mechanically, and SANDER will look for a `&qmmm` namelist with the details of the QM calculation.

In the `&qmmm` namelist, the atoms to be treated quantum mechanically are specified by `qmmask` (using the regular ambermask nomenclature, in this example, residues 1 to 3). `qmtheory=7` requests SCC-DFTB. All other flags are optional, and in this case use dispersion (`dftb_disper=1`) and request that CM3 charges be calculated and printed (`dftb_chg=1`), define the SCF convergence criterion (`scfconv=1.0e-9`), require that the same convergence criterion is to be used for the charges (`tight_p_conv=1`), and that the Ewald sum method is to be used for long-range electrostatics involving the QM atoms (`qm_ewald=1`). All the available options are described in more detail in the AMBER 9.0 manual. (<http://amber.scripps.edu>).

## Results and Discussion

Alanine dipeptide (Ace-Ala-NMe, henceforth abbreviated as AD, Figure 2) is a convenient model system, composed of

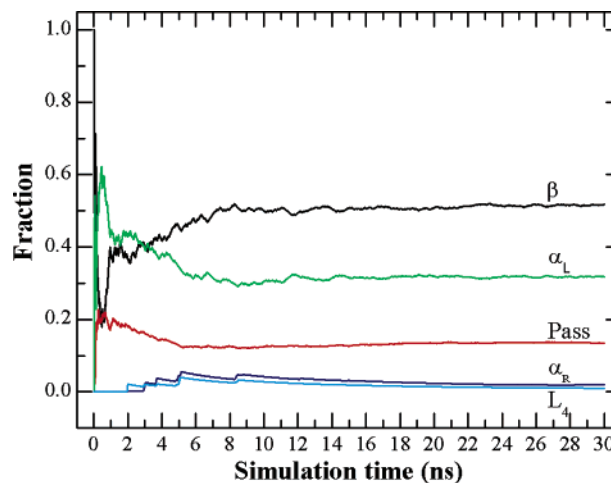


Figure 4. Convergence of the QM/MM simulation using  $1.0 \times 10^{-9} E_h$  convergence criterion. The regions in the Ramachandran plot are indicated in Figure 5.

an alanine unit blocked by an acetyl group at the N-terminus (Ace) and a *N*-methylamide group (NMe) at the C-terminus. It has often been used as a model system in studies of backbone conformational equilibrium in proteins. Recent experimental results suggest that the backbone preferences in proteins are already present in blocked aminoacids.<sup>55,56</sup> A number of experimental<sup>55,57-60</sup> and theoretical<sup>61-78</sup> studies indicate that the potential energy surface for AD in vacuum and in solution are considerably different: while in the gas-phase the global minimum is believed to be a  $C7_{eq}$  structure ( $\varphi \sim -83^\circ$ ,  $\psi \sim 73^\circ$ ),<sup>70</sup> interaction with water favors the polyproline-II ( $P_{II}$ ,  $\varphi \sim -75^\circ$ ,  $\psi \sim 150^\circ$ ) conformation.<sup>60</sup>

AD has also been used previously to investigate the performance of the SCC-DFTB method as compared to different classical force fields.<sup>69</sup> General force fields, being designed to reproduce the properties of large biological systems, have difficulty in the simulation of small molecules such as AD. On the other hand, high-level ab initio calculations are possible only for a small number of conformations and prohibitively expensive for extended molecular dynamics simulations.

To illustrate the use of SCC-DFTB in AMBER, two different applications are shown here: The first is a calculation of the free energy surface of AD in explicit water, where the AD is treated quantum mechanically and the water molecules classically using the TIP3P<sup>79</sup> model. Use of a fast semiempirical method (such as SCC-DFTB) coupled to a molecular mechanics representation of the solvent makes it possible to simulate the AD in water in a reasonable time scale. For comparison purposes, the same calculation is done where the AD is treated by a classical force field using the AMBER ff99SB<sup>9</sup> and ff03<sup>80,81</sup> parameters. The second example is an illustration of the use of advanced capabilities available in AMBER, a replica exchange molecular dynamics (REMD) simulation of AD in vacuum, where the whole AD is treated quantum mechanically. Those results are meant only to exemplify the use of SCC-DFTB in AMBER, and a more detailed study will be published elsewhere.

**Molecular Dynamics of Alanine Dipeptide in Explicit Water.** The system was prepared using the Leap program (part of the AMBER package). The AD solute was placed in a box with 630 water molecules for a total of 1912 atoms with periodic boundary conditions. All long-range interactions were calculated using the particle-mesh Ewald (PME) approach.<sup>52,82</sup> The SHAKE algorithm<sup>83,84</sup> was used to restrain the bonds containing hydrogen in both QM and MM regions, allowing a time step

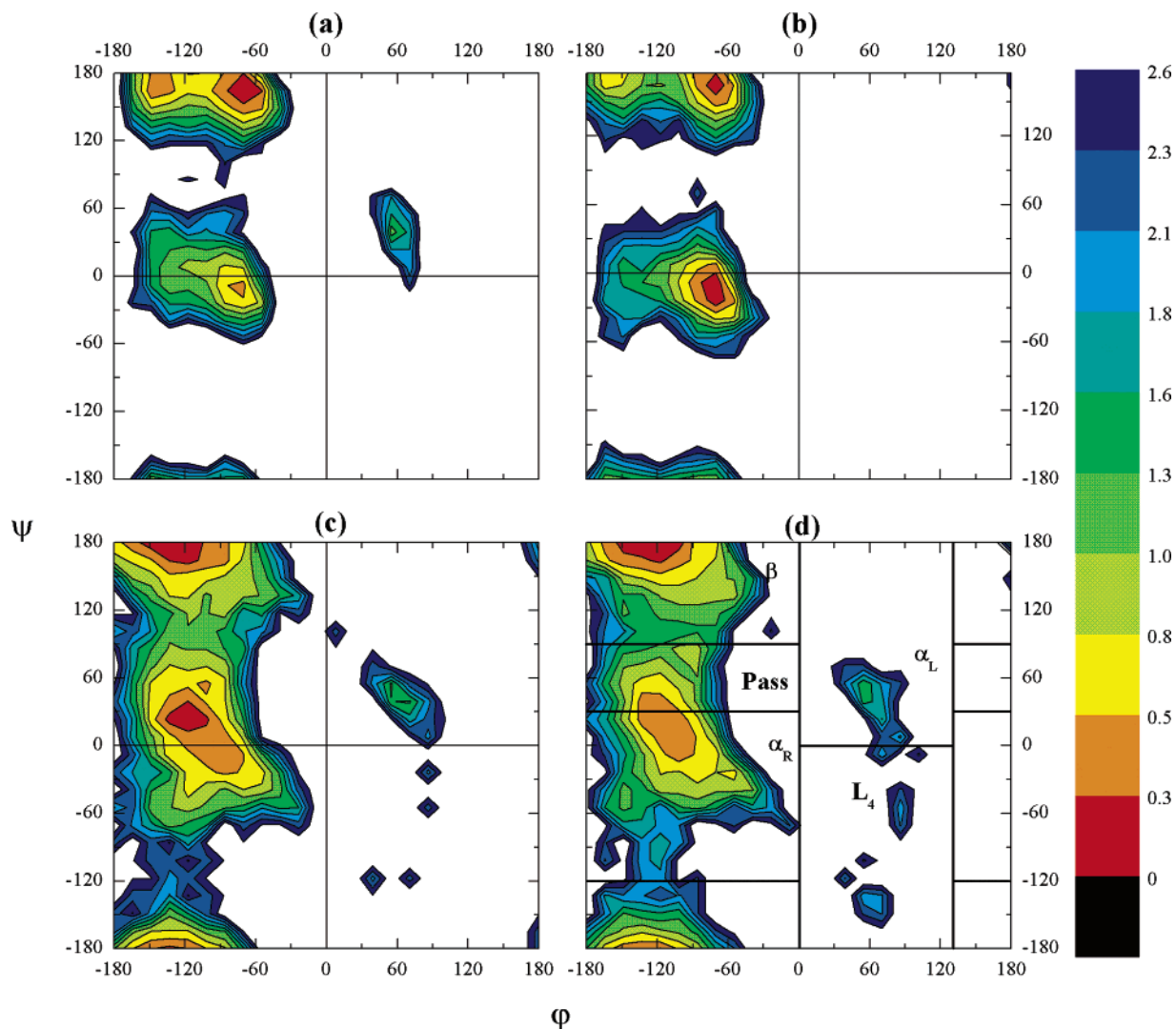


**Figure 5.** Free energy surfaces for alanine dipeptide in water, obtained using full classical calculations and the force fields (a) AMBER ff99SB, (b) AMBER ff03, and QM/MM (alanine dipeptide quantum, waters classical TIP3P) with SCF convergence tolerance set to (c)  $1.0 \times 10^{-6} E_h$ , (d)  $1.0 \times 10^{-9} E_h$ , and charge convergence criterion of  $0.05 \times (\text{SCF tolerance})^{1/2}$ . The divisions in (d) indicate the regions of the Ramachdran plot used in determining the convergence of the simulations (see Figure 4). The energy scale on the right side is in kcal/mol, relative to the global minimum in each case.

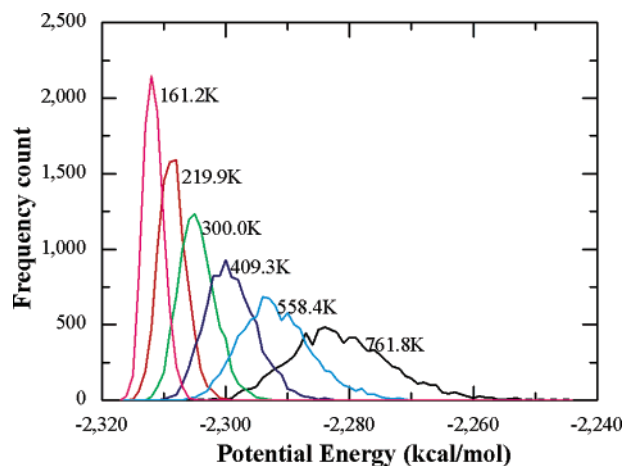


**Figure 6.** Potential energy distributions at the different temperatures used in the REMD simulation of alanine dipeptide.

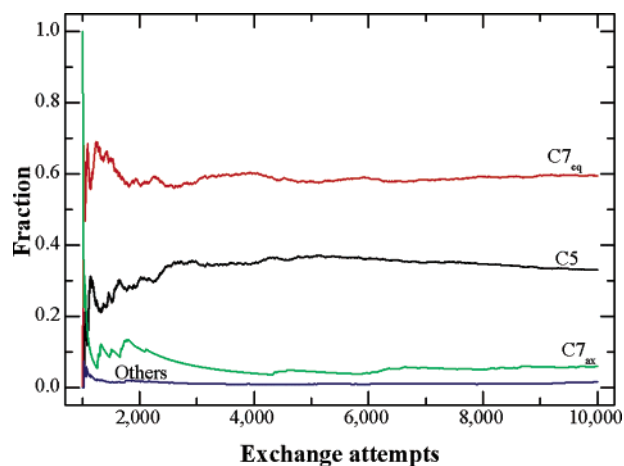


**Figure 7.** Convergence of the REMD simulation. The regions of the Ramachdran plot are indicated in Figure 8.

of 2 fs to be used. All constant temperature calculations used the Langevin thermostat<sup>85</sup> with a collision frequency of  $2.0 \text{ ps}^{-1}$ . Calculations with pressure regulation used a relaxation time of 2.0 ps. The QM/MM calculations used SCC-DFTB with

dispersion corrections for the AD (with the same dispersion parameters as published by Elstner et al.<sup>43</sup>) and the TIP3P model for the water molecules.<sup>79</sup> The van der Waals parameters from the classical force field AMBER ff99SB<sup>9</sup> were used for the

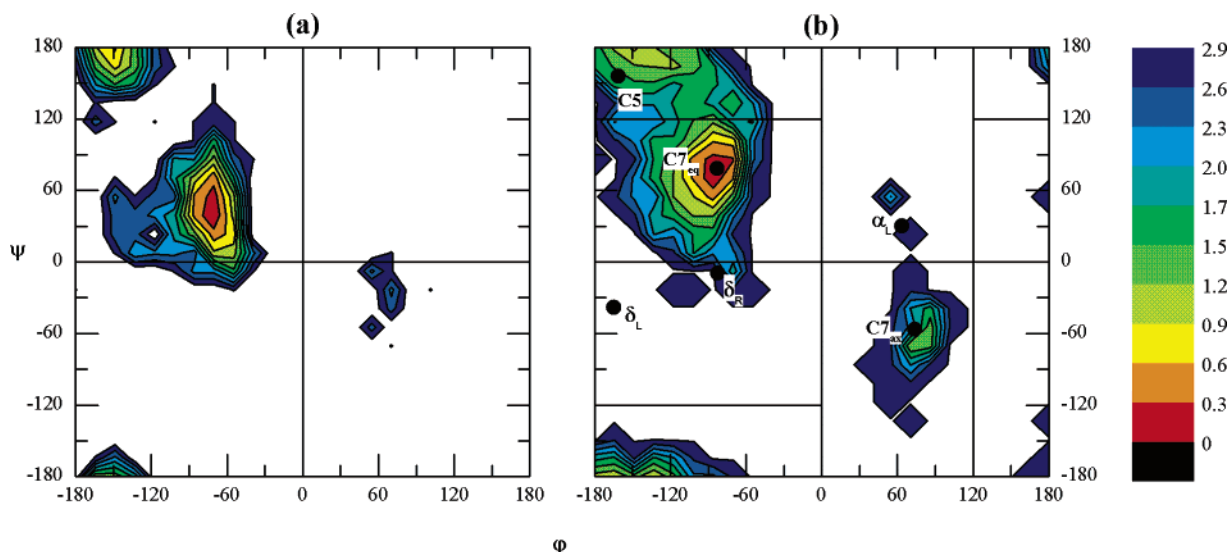


**Figure 8.** Free energy surface of alanine dipeptide in vacuum at 300 K, from the REMD simulations using QM and the AMBER ff99SB force field. The filled circles indicate the minima from Vargas et al.<sup>76</sup> The energy scale is in kcal/mol and relative to the global minimum in each case.

quantum atoms in the interaction with the classical region. For comparison purposes, similar calculations were performed with the AD treated quantum mechanically by the SCC-DFTB method and different convergence criteria, and also classically using the AMBER force fields ff99SB<sup>9</sup> and ff03.<sup>80,81</sup>

Before the production runs, all the systems were equilibrated. After a full MM energy minimization (to remove bad contacts), the system was run at 300 K for 100 ps using constant volume and temperature (*nVT*), then equilibrated to 1 bar pressure for another 100 ps using constant pressure and temperature (*nPT*). For the QM/MM calculations, an additional equilibration of 100 ps *nPT* with the AD now treated quantum mechanically was performed. All results shown here were generated after a production run of 30 ns at constant volume and energy (*nVE* ensemble), from which the first 10% are excluded from the analysis.

The SCF convergence criterion used was  $1.0 \times 10^{-9} E_h$  and the charges convergence criterion set to  $0.05 \times (\text{SCF tolerance})^{1/2}$  in all calculations. As a testament to the huge degree of optimization that has been undertaken while rewriting the DFTB code on a single processor, these calculations are just 2.6 and 2.9 times slower than an all-classical calculation. However, the current implementation is still not optimized for parallel processing, and the same calculations using four processors are 4.0 and 4.7 times slower than the all-classical calculation, respectively, indicating that most of the time is being spent on the classical calculations, which, in AMBER, are already parallelized. Extensive work is underway to make DFTB fully parallel in the next AMBER release, and it is anticipated that, by that time, the same DFTB calculations as above will be no more than 2.0 times slower than the corresponding all-classical simulation.

The total, kinetic, potential, and SCF energies vs time are shown in Figure 3. It can be clearly seen that energy is very well conserved on this time scale. Figure 4 shows the sampling convergence of this same calculation. The Ramachandran plot was divided in sections according to the previous work of Hu et al.,<sup>69</sup> (Figure 5d) and the number of structures in each session accumulated. It shows that indeed, the ensemble distribution has converged after 30 ns.

The free energy surfaces for AD were obtained by calculating the (normalized) probability  $P$  of finding the AD in a conformation at a particular region in  $(\varphi, \psi)$ -space from the MD

**TABLE 1:**  $(\varphi, \psi)$  Angles and Relative Energies for the Different Minima of Alanine Dipeptide, from Vargas et al. (ref 76)<sup>a</sup>

conformer	$\varphi$	$\psi$	$\Delta E$
C7 <sub>eq</sub>	-82.6	75.8	0.00
C <sub>5</sub>	-161.1	155.5	1.39
C7 <sub>ax</sub>	73.7	-53.7	2.66
$\delta_R$ ( $\beta_2$ )	-82.3	-9.5	3.35
$\alpha_L$	63.8	30.2	5.19
$\delta_L$ ( $\alpha'$ )	-164.7	-38.3	6.80

<sup>a</sup> Geometries were optimized at the MP2/aug-cc-pVDZ level and energies extrapolated to MP2/CBS limit. Angles are in deg, and energy differences in kcal/mol relative to the C7<sub>eq</sub> minimum.

trajectories, then converting this number to free energies by  $G = -RT \ln(P)$ , where  $G$  is the Gibbs free energy,  $R$  is the general gas constant, and  $T$  is the temperature. The free energy surfaces for AD in explicit water at 300 K calculated from the *nVE* trajectories are shown in Figure 5. To gauge the importance of tight convergence and thus more accurate gradients, results using a convergence criterion of  $1.0 \times 10^{-6} E_h$  in the SCF procedure are also shown. All surfaces show similar minima on the  $\beta$  and  $\alpha_R$  regions of the Ramachandran plot. However, the rotational barriers are higher in the classical calculations, especially in the simulations using the ff03 force field, an effect that may be related to the nature the harmonical approximation used by the force fields, as described above (eq 1). A similar conclusion was reached by Hu et al.<sup>69</sup> in a previous study.

Those surfaces can also be compared to the Ramachandran plots obtained by Lovell et al.<sup>86</sup> In that study, the authors searched the PDB database for the conformation of all peptides excluding glycine, proline, and pre-proline, and the structures found were arranged in a Ramachandran plot. Lovell et al. results<sup>86</sup> agree very well with the prediction from the QM trajectories displayed in Figure 5.

**Replica Exchange Molecular Dynamics of Alanine Dipeptide in Vacuum.** It is currently accepted that at least six minima exist in the energy surface of AD in vacuum, denoted by C7<sub>eq</sub>, C<sub>5</sub>, C7<sub>ax</sub>,  $\delta_R$ ,  $\alpha_L$ , and  $\delta_L$ , ordered from the most to the least stable structure according to ab initio and DFT calculations.<sup>35,64,67,70,76,77,87</sup> Although the relative energies change slightly, the overall ordering does not depend on the level of theory. Table 1 shows the dihedral angles and relative energies for these structures from Vargas et al.<sup>76</sup> The geometries were



optimized at the MP2/aug-cc-pVTZ level and the relative energies extrapolated to the complete basis set limit from a series of single point MP2/aug-cc-pV $\times$ Z calculations ( $x = D, T, Q$ ).<sup>76</sup>

For the REMD simulations of AD in vacuum, six replicas were used at temperatures of 161.2, 219.9, 300.0, 419.3, 558.4, and 761.8 K. Exchanges were attempted 10 000 times, with 0.5 ps between attempts, and a time step of 1 fs with SHAKE<sup>83,84</sup> was used. The Langevin thermostat<sup>85</sup> with a collision frequency of 2.0 ps<sup>-1</sup> was used to regulate the temperatures. The dispersion correction to the DFTB energy was applied in the same way as described above.

The potential energy distributions at the various temperatures used are shown in Figure 6. The overlap of the distributions indicates that the temperature distribution used was adequate. Figure 7 shows the sampling convergence of the REMD simulation as a function of the number of exchange attempts. The convergence was estimated as described above for AD in water by using the regions in the Ramachandran plot, as indicated in Figure 8. The plot in Figure 7 shows that the ensemble distribution obtained from the REMD calculation is converged.

The free energy surface obtained at 300 K is shown in Figure 8. The minima obtained by Vargas et al.<sup>76</sup> are also indicated for reference as filled circles. Note that the ab initio calculations only include enthalpy, while the results in Figure 8 represent free energies. Still, the concordance on the minima positions and energy ordering is excellent. It is important to notice, however, the slight displacement of the C5 minimum to a more extended structure. This overestimation of extended conformations with respect to helical ones has been noted for full DFT methods by Improtta and Barone<sup>70</sup> and is simply inherited by SCC-DFTB. For comparison purposes, the same calculation was done using the AMBER ff99SB<sup>9</sup> force field for the dipeptide, and the free energy surface is also shown in Figure 8. This force field was derived from the ff99 force field modified specifically to reproduce relative energy differences in alanine tetrapeptide (two more alanines than DA) from QM calculations. The free energy surface from the classical calculation does reproduce the basic features of the quantum surface but clearly cannot reproduce the expected minima positions correctly, and the same effect of higher rotational barriers (with respect to the quantum calculations) discussed above for the AD in water is seen here. Those results also highlight the importance of the inclusion of quantum effects in the calculation.

## Conclusions

This article shows the details of the implementation of SCC-DFTB in AMBER 9. Within the new design of AMBER 9's QM support, only a single keyword is needed to activate QM, and the details of the QM calculation are specified by QM-specific keywords in a simple, separate namelist. Efforts are currently under way to parallelize the SCC-DFTB code in AMBER. In a single processor, the present implementation is only 2–3 times slower than a full classical calculation for the systems studied.

Two example calculations were shown. One is a simple MD calculation of alanine dipeptide in explicit water. The second, illustrating the use of more advanced sampling methods available in AMBER, is the application of SCC-DFTB combined with replica-exchange molecular dynamics simulations for the calculation of the potential energy surface of the AD in vacuum. It was shown that the use of SCC-DFTB/AMBER calculations can reproduce the experimental or high-level energy surfaces with very good agreement.

This implementation has the advantage of blending seamlessly with a well-established MD program, opening the possibility to combine SCC-DFTB with any methods available in AMBER.

**Acknowledgment.** Computer resources were provided by the Large Allocations Resource Committee through grant TG-MCA05S010 to AER, the High-Performance Computing Center at the University of Florida and a local cluster built with a generous IBM-SUR grant. D.A.C. and R.C.W. acknowledge NIH Grant GM57513 for funding this work. R.C.W. and A.E.R. would like to thank the San Diego Supercomputer Center for their continued support of this project and future developments in Amber 10 through their Strategic Applications Collaboration program. The authors also thank Josh McClellan for very useful discussions, and Mike Crowley of The Scripps Research Institute for many helpful discussions and for assistance with the implementation.

## References and Notes

- (1) Allen, M. P.; Tildesley, D. J. *Computer Simulation of Liquids*; Oxford Science Publications: New York, 1987.
- (2) Michel, J.; Verdonk, M. L.; Essex, J. W. *J. Med. Chem.* **2006**, *49*, 7427.
- (3) Hornak, V.; Okur, A.; Rizzo, R. C.; Simmerling, C. *Proc. Natl. Acad. Sci. U.S.A.* **2006**, *103*, 915.
- (4) Basner, J. E.; Schwartz, S. D. *J. Am. Chem. Soc.* **2005**, *127*, 13822.
- (5) Simmerling, C.; Strockbine, B.; Roitberg, A. E. *J. Am. Chem. Soc.* **2002**, *124*, 11258.
- (6) Affentranger, R.; Tavernelli, I.; DiIorio, E. E. *J. Chem. Theory Comput.* **2006**, *2*, 217.
- (7) Caflisch, A.; Karplus, M. *Proc. Natl. Acad. Sci. U.S.A.* **1994**, *91*, 1746.
- (8) Case, D. A.; Cheatham, T. E., III; Darden, T.; Gohlke, H.; Luo, R.; Merz, K. M., Jr.; Onufriev, A.; Simmerling, C.; Wang, B.; Woods, R. *J. J. Comput. Chem.* **2005**, *26*, 1668.
- (9) Hornak, V.; Abel, R.; Okur, A.; Strockbine, B.; Roitberg, A.; Simmerling, C. *Proteins: Struct., Funct., Bioinform.* **2006**, *65*, 712.
- (10) Jono, R.; Shimizu, K.; Terada, T. *Chem. Phys. Lett.* **2006**, *432*, 306.
- (11) Hermans, J. *J. Phys. Chem. A* **2007**, *111*, 5685.
- (12) Borowski, T.; Georgiev, V.; Siegbahn, P. E. M. *J. Am. Chem. Soc.* **2005**, *127*, 17303.
- (13) Marothy, S. A. D.; Blomberg, M. R. A.; Siegbahn, P. E. M. *J. Comput. Chem.* **2007**, *28*, 528.
- (14) Warshel, A.; Levitt, M. *J. Mol. Biol.* **1976**, *103*, 227.
- (15) Field, M. J.; Bash, P. A.; Karplus, M. *J. Comput. Chem.* **1990**, *11*, 700.
- (16) Case, D. A.; Darden, T. A.; Cheatham, T. E., III; Simmerling, C. L.; Wang, J.; Duke, R. E.; Luo, R.; Merz, K. M.; Pearlman, D. A.; Crowley, M.; Walker, R. C.; Zhang, W.; Wang, B.; Hayik, S.; Roitberg, A.; Seabra, G.; Wong, K. F.; Paesani, F.; Wu, X.; Brozell, S.; Tsui, V.; Gohlke, H.; Yang, L.; Tan, C.; Mongan, J.; Hornak, V.; Cui, G.; Beroza, P.; Mathews, D. H.; Schafmeister, C.; Ross, W. S.; Kollman, P. A. *AMBER 9*, 9th ed.; University of California: San Francisco, 2006.
- (17) Dewar, M. J. S.; Thiel, W. *J. Am. Chem. Soc.* **1977**, *99*, 4899.
- (18) Dewar, M. J. S.; Thiel, W. *J. Am. Chem. Soc.* **1977**, *99*, 4907.
- (19) Dewar, M. J. S.; Zoebisch, E. G.; Healy, E. F.; Stewart, J. J. P. *J. Am. Chem. Soc.* **1985**, *107*, 3902.
- (20) Stewart, J. J. P. *J. Comput. Chem.* **1989**, *10*, 209.
- (21) Stewart, J. J. P. *J. Comput. Chem.* **1989**, *10*, 221.
- (22) Repasky, M. P.; Chandrasekhar, J.; Jorgensen, W. L. *J. Comput. Chem.* **2002**, *23*, 1601.
- (23) Thiel, W.; Voityuk, A. A. *J. Phys. Chem.* **1996**, *100*, 616.
- (24) Frauenheim, T.; Porezag, D.; Elstner, M.; Jungnickel, G.; Elsner, J.; Haugk, M.; Sieck, A.; Seifert, G. *Mat. Res. Soc. Symp. Proc.* **1998**, *491*, 91.
- (25) Elstner, M.; Porezag, D.; Jungnickel, G.; Elsner, J.; Haugk, M.; Frauenheim, T.; Suhai, S.; Seifert, G. *Phys. Rev. B: Condens. Matter* **1998**, *58*, 7260.
- (26) Walker, R. C.; Crowley, M. F.; Case, D. A. *J. Comput. Chem.* **2007**, in preparation.
- (27) Pengyu Ren, Ponder, J. W. *J. Comput. Chem.* **2002**, *23*, 1497.
- (28) Ren, P.; Ponder, J. W. *J. Phys. Chem. B* **2004**, *108*, 13427.
- (29) Riccardi, D.; Li, G.; Cui, Q. *J. Phys. Chem. B* **2004**, *108*, 6467.
- (30) Singh, U. C.; Kollman, P. A. *J. Comput. Chem.* **1986**, *7*, 718.
- (31) Bersuker, I. B.; Leong, M. K.; Boggs, J. E.; Pearlman, R. S. *Int. J. Quantum Chem.* **1997**, *63*, 1051.

- (32) Maseras, F.; Morokuma, K. *J. Comput. Chem.* **1995**, *16*, 1170.
- (33) Zhang, Y. K.; Lee, T. S.; Yang, W. T. *J. Chem. Phys.* **1999**, *110*, 46.
- (34) Gao, J. L.; Amara, P.; Alhambra, C.; Field, M. J. *J. Phys. Chem. A* **1998**, *102*, 4714.
- (35) Philipp, D. M.; Friesner, R. A. *J. Comput. Chem.* **1999**, *20*, 1468.
- (36) Field, M. J.; Albe, M.; Bret, C.; Proust-De Martin, F.; Thomas, A. *J. Comput. Chem.* **2000**, *21*, 1088.
- (37) Konig, P. H.; Hoffmann, M.; Frauenheim, T.; Cui, Q. *J. Phys. Chem. B* **2005**, *109*, 9082.
- (38) Porezag, D.; Frauenheim, T.; Köhler, T.; Seifert, G.; Kaschner, R. *Phys. Rev. B* **1995**, *51*, 12947.
- (39) Eschrig, H.; Bergert, I. *Phys. Status Solidi B* **1978**, *90*, 621.
- (40) Elstner, M. *Theor. Chim. Acta.* **2006**, *116*, 316.
- (41) Kristyan, S.; Pulay, P. *Chem. Phys. Lett.* **1994**, *229*, 175.
- (42) Perez-Jorda, J.; Becke, A. D. *Chem. Phys. Lett.* **1995**, *233*, 134.
- (43) Elstner, M.; Hobza, P.; Frauenheim, T.; Suhai, S.; Kaxiras, E. *J. Chem. Phys.* **2001**, *114*, 5149.
- (44) Zhechkov, L.; Heine, T.; Patchkovskii, S.; Seifert, G.; Duarte, H. A. *J. Chem. Theory Comput.* **2005**, *1*, 841.
- (45) Mitsutake, A.; Sugita, Y.; Okamoto, Y. *Pept. Sci.* **2001**, *60*, 96.
- (46) Schlitter, J.; Engels, M.; Kruger, P. *J. Mol. Graph.* **1994**, *12*, 84.
- (47) Schlitter, J.; Swegat, W.; Mülders, T. *J. Mol. Model.* **2001**, *7*, 171.
- (48) Winget, P.; Thompson, J. D.; Xidos, J. D.; Cramer, C. J.; Truhlar, D. G. *J. Phys. Chem. A* **2002**, *106*, 10707.
- (49) Kalinowski, J. A.; Lesyng, B.; Thompson, J. D.; Cramer, C. J.; Truhlar, D. G. *J. Phys. Chem. A* **2004**, *108*, 2545.
- (50) Ewald, P. P. *Ann. Phys. (Leipzig)* **1921**, *369*, 253.
- (51) Nam, K.; Gao, J.; York, D. M. *J. Chem. Theory Comput.* **2005**, *1*, 2.
- (52) Darden, T.; York, D.; Pedersen, L. *J. Chem. Phys.* **1993**, *98*, 10089.
- (53) Xie, L.; Liu, H. *J. Comput. Chem.* **2002**, *23*, 1404.
- (54) Pellegrini, E.; Field, M. J. *J. Phys. Chem. A* **2002**, *106*, 1316.
- (55) Avbelj, F.; Grdadolnik, S. G.; Grdadolnik, J.; Baldwin, R. L. *Proc. Natl. Acad. Sci. U.S.A.* **2006**, *103*, 1272.
- (56) Shi, Z.; Chen, K.; Liu, Z.; Ng, A.; Bracken, W. C.; Kallenbach, N. R. *Proc. Natl. Acad. Sci. U.S.A.* **2005**, *102*, 17964.
- (57) Kang, Y. K. *J. Phys. Chem. B* **2006**, *110*, 21338.
- (58) Kim, Y. S.; Wang, J.; Hochstrasser, R. M. *J. Phys. Chem. B* **2005**, *109*, 7511.
- (59) Lavrich, R. J.; Plusquellic, D. F.; Suenram, R. D.; Fraser, G. T.; Walker, A. R. H.; Tubergen, M. J. *J. Chem. Phys.* **2003**, *118*, 1253.
- (60) Poon, C. D.; Samulski, E. T.; Weise, C. F.; Weisshaar, J. C. *J. Am. Chem. Soc.* **2000**, *122*, 5642.
- (61) Smith, P. E. *J. Chem. Phys.* **1999**, *111*, 5568.
- (62) Aleman, C.; Leon, S. *J. Mol. Struct. THEOCHEM.* **2000**, *505*, 211.
- (63) Apostolakis, J.; Ferrara, P.; Caflich, A. *J. Chem. Phys.* **1999**, *110*, 2099.
- (64) Beachy, M. D.; Chasman, D.; Murphy, R. B.; Halgren, T. A.; Friesner, R. A. *J. Am. Chem. Soc.* **1997**, *119*, 5908.
- (65) Boresch, S.; Willensdorfer, M.; Steinhauser, O. *J. Chem. Phys.* **2004**, *120*, 3333.
- (66) Cui, Q.; Elstner, M.; Kaxiras, E.; Frauenheim, T.; Karplus, M. *J. Phys. Chem. B* **2001**, *105*, 569.
- (67) Elstner, M.; Jalkanen, K. J.; Knapp-Mohammady, M.; Frauenheim, T.; Suhai, S. *Chem. Phys.* **2001**, *263*, 203.
- (68) Han, W.-G.; Jalkanen, K. J.; Elstner, M.; Suhai, S. *J. Phys. Chem. B* **1998**, *102*, 2587.
- (69) Hu, H.; Elstner, M.; Hermans, J. *Proteins: Struct. Funct., Genet.* **2003**, *50*, 451.
- (70) Improta, R.; Barone, V. *J. Comput. Chem.* **2004**, *25*, 1333.
- (71) Iwaoka, M.; Okada, M.; Tomoda, S. *J. Mol. Struct. THEOCHEM.* **2002**, *586*, 111.
- (72) Kalko, S. G.; Guardia, E.; Padro, J. A. *J. Phys. Chem. B* **1999**, *103*, 3935.
- (73) Liu, P.; Kim, B.; Friesner, R. A.; Berne, B. J. *Proc. Natl. Acad. Sci. U.S.A.* **2005**, *102*, 13749.
- (74) Marrone, T. J.; Gilson, M. K.; McCammon, J. A. *J. Phys. Chem.* **1996**, *100*, 1439.
- (75) Tobias, D. J.; Brooks, C. L. *J. Chem. Phys.* **1992**, *96*, 3864.
- (76) Vargas, R.; Garza, J.; Hay, B. P.; Dixon, D. A. *J. Phys. Chem. A* **2002**, *106*, 3213.
- (77) Wei, D.; Guo, H.; Salahub, D. R. *Phys. Rev. E* **2001**, *64*, 011907/1.
- (78) Wang, Z.-X.; Duan, Y. *J. Comput. Chem.* **2004**, *25*, 1699.
- (79) Jorgensen, W. L.; Chandrasekhar, J.; Madura, J. D.; Impey, R. W.; Klein, M. L. *J. Chem. Phys.* **1983**, *79*, 926.
- (80) Duan, Y.; Wu, C.; Chowdhury, S.; Lee, M. C.; Xiong, G.; Zhang, W.; Yang, R.; Cieplak, P.; Luo, R.; Lee, T.; Caldwell, J.; Wang, J.; Kollman, P. *J. Comput. Chem.* **2003**, *24*, 1999.
- (81) Lee, M. C.; Duan, Y. *Proteins: Struct., Funct., Bioinform.* **2004**, *55*, 620.
- (82) Essmann, U.; Perera, L.; Berkowitz, M. L.; Darden, T.; Lee, H.; Pedersen, L. G. *J. Chem. Phys.* **1995**, *103*, 8577.
- (83) Ryckaert, J.-P.; Ciccotti, G.; Berendsen, H. J. C. *J. Comput. Phys.* **1977**, *23*, 327.
- (84) Miyamoto, S.; Kollman, P. A. *J. Comput. Chem.* **1992**, *13*, 952.
- (85) He, S.; Scheraga, H. A. *J. Chem. Phys.* **1998**, *108*, 271.
- (86) Lovell, S. C.; Davis, I. W.; Arendall, W. B., III; de Bakker, P. I.; Word, J. M.; Prisant, M. G.; Richardson, J. S.; Richardson, D. C. *Proteins: Struct., Funct., Genet.* **2003**, *50*, 437.
- (87) Perczel, A.; Farkas, O.; Jakli, I.; Topol, I. A.; Csizmadia, I. G. *J. Comput. Chem.* **2003**, *24*, 1026.